Quaternary Science Reviews 88 (2014) 135–146

Contents lists available at ScienceDirect

Quaternary Science Reviews

journal homepage: www.elsevier.com/locate/quascirev

Age through tandem correlation of Quaternary relative paleointensity (RPI) and oxygen isotope data at IODP Site U1306 (Eirik Drift, SW Greenland)

J.E.T. Channell [a,*], J.D. Wright [b], A. Mazaud [c], J.S. Stoner [d]

[a] Department of Geological Sciences, University of Florida, POB 112120, Gainesville, FL 32611, USA
[b] Department of Earth and Planetary Sciences, Rutgers University, Piscataway, NJ 08854, USA
[c] Laboratoire des Sciences du Climat et de l'Environnement, CEA-CNRS, Gif-sur-Yvette, France
[d] College of Oceanic and Atmospheric Sciences, Oregon State University, Corvallis, OR, USA

ARTICLE INFO

Article history:
Received 5 November 2013
Received in revised form
30 January 2014
Accepted 31 January 2014
Available online

Keywords:
Eirik drift
North Atlantic
Quaternary
Relative paleointensity
Oxygen isotopes
Deep Western Boundary Current

ABSTRACT

Planktic oxygen isotope ($\delta^{18}O$) and relative paleointensity (RPI) data are used in tandem to generate an age model for the last 1 Myr from Integrated Ocean Drilling Program (IODP) Site U1306 drilled on the crest of the Eirik Drift (SW Greenland) in 2272 m water depth. For the 1–1.5 Ma interval, the age model is based on RPI alone due to insufficient foraminifera for isotope analyses. Utilizing RPI and $\delta^{18}O$ in tandem allows recognition of low-$\delta^{18}O$ "events" prior to glacial Terminations I, III, IV, V, VII, VIII, IX and X, that are independently supported by radiocarbon dates through the last deglaciation, and are attributed to local or regional surface-water effects. At Site U1306, Quaternary sedimentation rates (mean ~15 cm/ka) are elevated during peak glacials and glacial onsets, and are reduced during interglacials, in contrast to the pattern at Site U1305 in 3460 m water depth at the distal toe of the drift, 191 km SW of Site U1306. The contrasting sedimentation-rate pattern appears to hold for the entire ~1.5 Myr record. The slackening and/or shoaling (due to lowered salinity) of the Deep Western Boundary Current (DWBC) during glacial intervals coincided with greater sediment supply to Site U1306 whereas the deepening, and possibly increased vigor, of the DWBC during interglacial intervals boosted sediment supply to Site U1305.

1. Introduction

The Deep Western Boundary Current (DWBC), commonly referred to as the Western Boundary Undercurrent (WBUC) (e.g., Arthur et al., 1989), sweeps southward off eastern Greenland at ~2000–3000 m water depth (Fig. 1). Carrying an important (~6–12 Sv) component of North Atlantic Deep Water (NADW), the DWBC is presently dominated by Denmark Strait Overflow Water (DSOW), and is therefore an important component of Atlantic Meridional Overturning Circulation (AMOC) (Bacon, 1997; Hunter et al., 2007a, b; Holliday et al., 2009; Bacon and Saunders, 2010; Stanford et al., 2011). Eirik Drift, commonly referred to as the Eirik Ridge, was built off SE Greenland (Fig. 1) since Late Miocene (Arthur et al., 1989) by DWBC interaction with bathymetry as it flowed around the southern tip of Greenland (Holliday et al., 2009). The crest of the Eirik Drift deepens from ~1500 m water depth close to Cape Farewell (Greenland) to >3400 m at the toe of the drift to the SW, over a distance of ~350 km (Fig. 1). Based on a few piston cores, the depositional pattern on Eirik Drift over the last climate cycle depends on location, with elevated interglacial sedimentation rates close to the toe of the drift at water depths in excess of ~3000 m, and relatively elevated sedimentation rates during the last glacial at water depths <2500 m (Hillaire-Marcel et al., 1994; Stoner et al., 1995, 1998; Evans et al., 2007).

Integrated Ocean Drilling Program (IODP) Site U1306 (58.24°N, 45.64°W) and Site U1305 (57.48°N, 48.53°W) are located on Eirik Drift in water depths of 2272 m and 3460 m, respectively (Fig. 1), and are separated by 191 km. The sites are suitably located to monitor depositional variability through the Quaternary at the distal toe (Site U1305) and proximal lee-side crest of the drift (Site U1306). The sites were chosen based on interpretation of seismic stratigraphy, partly acquired during cruise KN166-14 of R/V *Knorr* in summer 2002, that implied relatively expanded Quaternary sedimentary sections at both sites (Channell et al., 2006).

The modern configuration of erosion and deposition on Eirik Drift has been inferred from hydrographic data and 3.5/5.1 kHz

* Corresponding author. Tel.: +1 352 392 3658; fax: +1 352 392 9294.
E-mail address: jetc@ufl.edu (J.E.T. Channell).

http://dx.doi.org/10.1016/j.quascirev.2014.01.022
0277-3791/

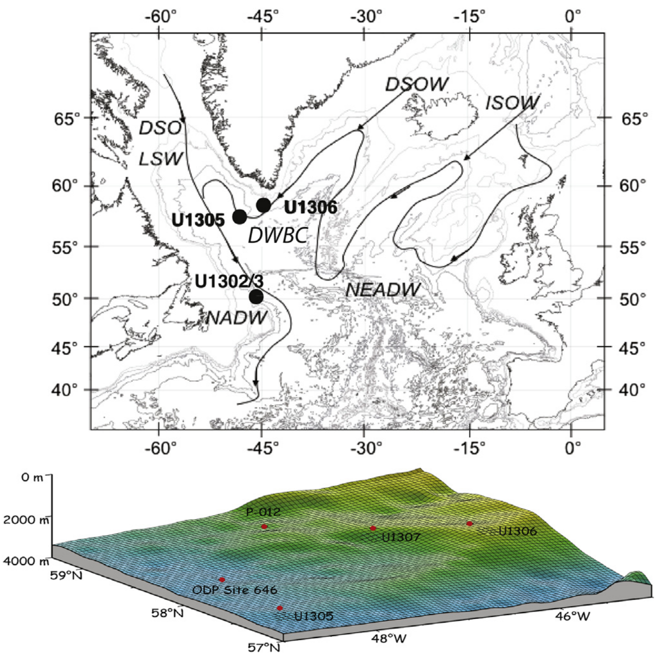

Fig. 1. Location map for IODP Sites U1306, U1305 on Eirik Drift off southern Greenland (Cape Farewell) and IODP Site U1302/3 (Orphan Knoll), and (below) their location relative to ODP Site 646, IODP Site U1307 and Core HU90-013-012 (P-012). Principal ocean currents are indicated by arrows: Denmark Strait Overflow Water (DSOW), Labrador Sea Water (LSW), Iceland–Scotland Overflow Water (ISOW), North East Atlantic Deep Water (NEADW), Deep Western Boundary Current (DWBC), Davis Straight Overflow Water (DSO), and North Atlantic Deep Water (NADW). Maps modified after Mazaud et al. (2012) and Channell et al. (2006).

profiler lines, from which the acoustic character of surface sediment can be interpreted in terms of erosion/deposition related to the role of the DWBC (Hunter et al., 2007a). Although the characteristics of the DWBC may vary on decadal and millennial timescales (e.g., Fagel et al., 2004; Bacon and Saunders, 2010), the modern pattern is dominated by erosion on the eastern side of the drift, in the ~2000–3000 m water depth range where the DWBC is most active, and by deposition at the toe of the drift in the vicinity of Site U1305 (Fig. 1). The DWBC probably shoaled and slowed during glacial intervals (e.g., Hall and Becker, 2007) thereby reducing detrital deposition during glacials, relative to interglacials, at Site U1305 (Hillaire-Marcel et al., 2011). The near-surface currents in the region, the East Greenland Current (EGC) and the East Greenland Coastal Current (EGCC), may play a subsidiary role in supplying detritus, particularly to the lee (western) side of the drift crest.

Shipboard magnetic stratigraphies for IODP Sites U1306 and U1305 have high fidelity and indicate that the recovered ~300 m sedimentary sequences at both sites reach back to the Olduvai Subchron at ~2 Ma, implying mean sedimentation rates of ~15 cm/ka (Expedition 303 Scientists, 2006a,b). At Site U1305, planktic oxygen isotope data ($\delta^{18}O$) based on *Neogloboquadrina pachyderma* (sin.) extend back to marine isotope stage (MIS) 33 at ~1.1 Ma (Hillaire-Marcel et al., 2011). The magnetic polarity stratigraphy and the record of geomagnetic relative paleointensity (RPI) at Site U1305 reaches into the Matuyama Chron, just beyond the onset of the Jaramillo Subchron at ~1.1 Ma (Mazaud et al., 2012).

In this paper, we report the paleomagnetic record, comprising both directional and RPI data, and the planktic oxygen isotope ($\delta^{18}O$) record based on *N. pachyderma* (sin.), from Site U1306. We utilize the planktic oxygen isotope and the RPI records in tandem to derive an age model, thereby providing a test of tandem correlations of RPI and $\delta^{18}O$ to independent calibrated templates as a tool for improving the resolution of Quaternary stratigraphy. We then compare the Site U1306 age model with the published age model for Site U1305, in order to resolve depositional patterns at the two sites, and hence shed light on the Quaternary evolution of Eirik Drift and of the DWBC.

For Quaternary deep-sea sediments, oxygen isotope ($\delta^{18}O$) stratigraphies provide the traditional means of temporal calibration (age control). Age models are often developed through correlations to calibrated reference records (e.g., LR04 of Lisiecki and Raymo, 2005), usually through ties at glacial–interglacial transitions (terminations) and elsewhere. At high latitudes proximal to large Quaternary ice sheets (e.g., on the Eirik Drift), planktic $\delta^{18}O$ may be strongly perturbed by ice advances that bring light $\delta^{18}O$ from continental ice into contact with sea water, meltwater events, and the production of isotopically light brines due to sea-ice growth (Hillaire-Marcel and de Vernal, 2008). Offsets of a few thousand years in matching $\delta^{18}O$ records to templates are likely at terminations, as their position can be significantly perturbed by local variations in water temperature, salinity and chemistry, particularly for planktic $\delta^{18}O$ but also for benthic $\delta^{18}O$ (Skinner and Shackleton, 2005; Lisiecki and Raymo, 2009). RPI data have been shown to be useful for long-distance stratigraphic correlation, and can be used in conjunction with oxygen isotope data to produce tandem correlations that utilize both (ostensibly) global signals to improve Quaternary stratigraphy (e.g., Channell et al., 2009).

2. Methods

The natural remanent magnetization (NRM) of sediments at Site U1306 was measured on u-channel samples collected from archive halves of the composite splice, compiled shipboard from the four holes drilled at the site (Expedition 303 Scientists, 2006a,b). The composite splice extends to 215 m composite depth (mcd). U-channel samples, which are continuous samples with a square 2×2 cm cross-section encased in plastic, were collected from each (150 cm) core section within the composite splice. The advantage of u-channel measurements over shipboard data includes the reduced influence of drilling disturbance, improved measurement resolution due to magnetometer design, and the ability to carry out complete AF demagnetization to isolate magnetization components and impart laboratory magnetizations to develop RPI proxies. The RPI record derived from u-channel samples at Site U1306 extends back to 1.5 Ma, and is accompanied by a polarity stratigraphy in which the Matuyama-Brunhes boundary and the boundaries of the Jaramillo and Cobb Mountain subchronozones are identified.

U-channel measurements were carried out at 1-cm spacing, with a 10-cm leader and trailer on a 2G Enterprises magnetometer at the University of Florida. The archive halves were demagnetized shipboard at peak fields of 20 mT, therefore, the measurement protocol for u-channels comprised initial NRM measurement prior to u-channel demagnetization, then measurement after demagnetization at peak fields of 20–60 mT, applied in 5 mT increments, followed by peak fields of 60–100 mT applied in 10 mT increments. Magnetization components were computed for the 20–80 mT peak-field interval without anchoring to the origin of the orthogonal projections using standard methods (Kirschvink, 1980) and the UPmag software (Xuan and Channell, 2009). The component magnetizations, computed at 1-cm intervals, are associated with maximum angular deviation (MAD) values that gauge the quality of individual component directions with values $<10°$ representing adequate precision.

The relative strength of the geomagnetic field, or relative paleointensity (RPI), at the time of sediment deposition can be estimated by using the intensity of different types of laboratory-induced magnetizations, including anhysteretic remanent magnetization (ARM) and isothermal remanent magnetization (IRM), to normalize the natural remanent magnetization (NRM) intensity for changes in concentration of NRM-carrying grains (Banerjee and Mellema, 1974; Levi and Banerjee, 1976; King et al., 1983; Tauxe, 1993). Our procedure for measuring RPI proxies involved NRM demagnetization, followed by initial ARM acquisition in a 100 mT peak alternating field (and 50 μT DC bias field). After demagnetization of the initial ARM, ARM was reacquired stepwise in peak alternating fields up to 100 mT (in a 50 μT bias field), followed by IRM acquisition in a 1 T field and subsequent IRM demagnetization. We use the same demagnetization/acquisition peak alternating fields for ARM and IRM, as for NRM demagnetization. We then calculate three slopes for the 20–60 mT peak field demagnetization/acquisition interval that constitute the RPI proxies (Channell et al., 2002, 2008): slopes of NRM-lost versus (1) ARM-lost, (2) ARMAQ (ARM acquisition) and (3) IRM-lost. These three slopes, determined over specific demagnetization (acquisition) intervals using the UPmag software (Xuan and Channell, 2009), are analogous to calculating the NRM/ARM, NRM/ARMAQ and NRM/IRM ratios, and are accompanied by linear correlation coefficients (r) that yield the linearity (precision) of each slope, calculated at 1-cm intervals down-core.

After NRM demagnetization, and before ARM acquisition, volume susceptibility (κ) was measured at 1-cm intervals using a susceptibility bridge designed for u-channel samples that utilizes a 3-cm-sided square-shaped Sapphire Instruments loop sensor (Thomas et al., 2003). Anhysteretic susceptibility (κ_{ARM}) is then calculated by dividing the ARM intensity by the biasing DC field (50 μT) used to acquire the ARM. Following King et al. (1983), we used the ratio of anhysteretic susceptibility (κ_{ARM}) to susceptibility (κ) as a magnetite grain size proxy. The S-ratio was calculated, each 1-cm from u-channel samples, as IRM intensity acquired in a 0.3 T DC field divided by a subsequent IRM acquired in a 1 T DC field. The S-ratio can be used to ascertain the importance of high-coercivity magnetic minerals such as hematite and goethite.

In addition, we use a Princeton Measurements Corporation vibrating sample magnetometer (VSM) to determine hysteresis ratios: M_r/M_s and H_{cr}/H_c, where M_r is saturation remanence, M_s is saturation magnetization, H_{cr} is coercivity of remanence, and H_c is coercive force. Hysteresis ratios can be used to delineate single domain (SD), pseudo-single domain (PSD) and multidomain (MD) magnetite and assign "mean" magnetite grain sizes through empirical and theoretical calibrations of the so-called Day plot (Day et al., 1977; Carter-Stiglitz et al., 2001; Dunlop, 2002; Dunlop and Carter-Stiglitz, 2006). Magnetic hysteresis properties were also analyzed using first-order reversal curve (FORC) diagrams that provide enhanced mineral and domain state discrimination (Pike et al., 1999; Roberts et al., 2000; Muxworthy and Roberts, 2007). FORCs are measured by progressively saturating a small (few hundred mg) sample in a field (H_{sat}), decreasing the field to a value H_a, reversing the field and sweeping it back to H_{sat} in a series of regular field steps (H_b). The process is repeated for many values of H_a. The FORC diagram is a contour plot with axes B_c and B_u where $B_c=(H_b-H_a)/2$ and $B_u=(H_b + H_a)/2$. The contoured FORC distribution can be interpreted in terms of the coercivity distribution along the B_c axis. Spreading of the distribution along the B_u axis corresponds to magnetostatic interactions for SD grains or, more commonly in pelagic sediments, internal demagnetizing fields for MD grains. In general, closed peaked structures along the B_c axis are characteristic of SD gains, with contours becoming progressively more parallel to the B_u axis with grain-size coarsening. FORC diagrams were analyzed using the software of Harrison and Feinberg (2008) with smoothing factors of 6, measurement averaging time of 1 s, and a field increment of 2 mT up to a maximum applied field of 1 T.

IRM acquisition curves were generated using the VSM. The IRM was measured at one hundred magnetizing field steps, interpolated to be uniformly spaced on a logarithmic scale from ~7 mT to 1 T. The IRM acquisition curves were then analyzed for coercivity components using the IRM-UNMIXER software (Heslop et al., 2002) that relies on the supposition of Robertson and France (1994) that, in the absence of magnetic interactions, the first derivatives of IRM acquisition curves yield log-normal probability density functions that represent coercivity spectra.

For transmission electron microscopy (TEM), a single magnetic extract was prepared from a core section (1306C-2H-6) at 9.5 mcd (MIS3/4 boundary) by sonicating ~20 cm^3 of sediment in a sodium metaphosphate dispersant. The solution was loaded into a reservoir feeding a circulating system driven by a peristaltic pump that allowed the fluid to pass slowly, without turbulence, past the outside of a test-tube containing a rare-earth magnet. The material that adhered to the outside of the test-tube was then removed to a methanol solution using a methanol squeeze-bottle. Grains of magnetic separate were encouraged to adhere to a 3 mm TEM grid using another magnet suspended a few cm above the floating grid. Observations were made using a JEOL JEM-2010F high-resolution (HR) TEM in conjunction with energy dispersive X-ray spectroscopy (EDS) at an accelerating voltage of 200 kV. The microscope is equipped with a Gatan MultiScan Camera Model 794 for imaging and an Oxford Instruments detector with INCA 4.05 software for microanalysis. Spot analysis and line-scans were conducted in STEM mode with a nominally ~1 nm probe size and a camera length of 12 cm.

The oxygen isotope ($\delta^{18}O$) stratigraphy at Site U1306 is based on planktic foraminifera (*N. pachyderma*, sin.) and extends back to marine isotope stage (MIS) 27 at ~1 Ma. The rarity of benthic foraminifera at this site makes it impractical to establish a continuous benthic isotope record. *N. pachyderma* (s) is a polar species, which inhabits depths just below the surface mixed layer in open ocean environments (e.g., Bé and Tolderlund, 1971) and is the dominant planktic foraminiferal taxon in both glacial and interglacial intervals at Site U1306. Dried sediment samples were weighed and washed through a 63-μm sieve using tap water. Samples were then ultrasonically cleaned in distilled water for 3–5 s. We used an average of 10 specimens (about 60 μg) picked from the 150–250 μm size fraction. The shells were reacted at 90 °C with >100% orthophosphoric acid, using a "multiprep" device online with a Fisons Optima mass spectrometer. The standards included NBS-19 (Coplen, 1996) and the in-house RGF carbonate standard at Rutgers University that is routinely measured with NBS-18 and NBS-19. The 1-sigma standard deviations from replicate standard measurements (minimum of 8 standards during each run) are routinely 0.04 and 0.07‰ for $\delta^{13}C$ and $\delta^{18}O$, respectively. Samples were analyzed at 5-cm intervals down-core to a core depth of 156 mcd corresponding to an age of ~1.0 Ma. Results are reported as δ-values against VPDB (Coplen, 1996). Below 156 mcd, samples were usually barren of foraminifers.

As for $\delta^{18}O$, RPI proxies can also be perturbed by environmental/lithological variability. For this reason, we do not use RPI alone to generate the age model, but tandem correlation of both RPI and $\delta^{18}O$ to calibrated templates. We are thereby utilizing two ostensibly independent global signals to optimize the age model. The calibrated templates for $\delta^{18}O$ and RPI are the LR04 benthic oxygen isotope stack (Lisiecki and Raymo, 2005) and PISO-1500 (Channell et al., 2009), respectively. The tandem correlations are performed using a version of the *Match* protocol of Lisiecki and Lisiecki (2002). At Sites U1306, the RPI record extends beyond the $\delta^{18}O$ record and for this interval the age model relies on the *Match* correlation of RPI to PISO, rather than tandem correlation. We use polarity reversals (Fig. 2) as age-ties in the *Match* protocol with "penalties" that discourage departure from their established ages. The procedure allows introduction of penalty functions that limit sedimentation rate changes within records. There is a disadvantage in imposing this limitation because hiatuses and short-term deposition can occur, however, the penalty functions are set as broad as practical to obtain useful results. The advantage of *Match* over purely visual correlations is that the process is repeatable, and is based on explicit criteria. Data preparation for *Match* application involves scaling each record to zero mean and one standard deviation, and dividing each record into intervals, equivalent to ~1 ka in our case. Similar tandem correlation methods have been used to generate age models at IODP Site 1302/3 (Fig. 1), located at Orphan Knoll off Newfoundland, and at ODP Site 1063 on Bermuda Rise (Channell et al., 2012a, b).

Thirteen AMS radiocarbon ages from nine stratigraphic levels are available for the 6–31 ka interval of the tandem age model. All analyses were performed at the W. M. Keck Carbon Cycle Accelerator Mass Spectrometry Laboratory at UC Irvine (Table 1). Ages were derived from specimens of *N. pachyderma* (sin.), and corrected using a constant reservoir age of 400 yrs following Butzin et al. (2005). The reservoir-corrected ^{14}C ages were converted to calendar ages using the Fairbanks et al. (2005) calibration.

3. Magnetic properties and TEM observations

Shipboard pass-through paleomagnetic measurements at Site U1306 were made on archive half-cores at 5-cm intervals after one or two demagnetizing steps at peak fields not exceeding 20 mT (Expedition 303 Scientists, 2006a). Component magnetization directions for the 20–80 mT peak field demagnetization interval, determined post-cruise from u-channel samples, are well defined being associated with MAD values below 5° (Fig. 2). MAD values exceed 10° in some intervals (Fig. 2), particularly in the vicinity of polarity reversals and apparent magnetic excursions (the evidence for magnetic excursions at this site will be the subject of a subsequent paper). MAD values could be lowered by choosing demagnetization ranges for individual component directions, however, calculation for a global (20–80 mT) demagnetization range, and accompanying MAD values, allows a more straightforward

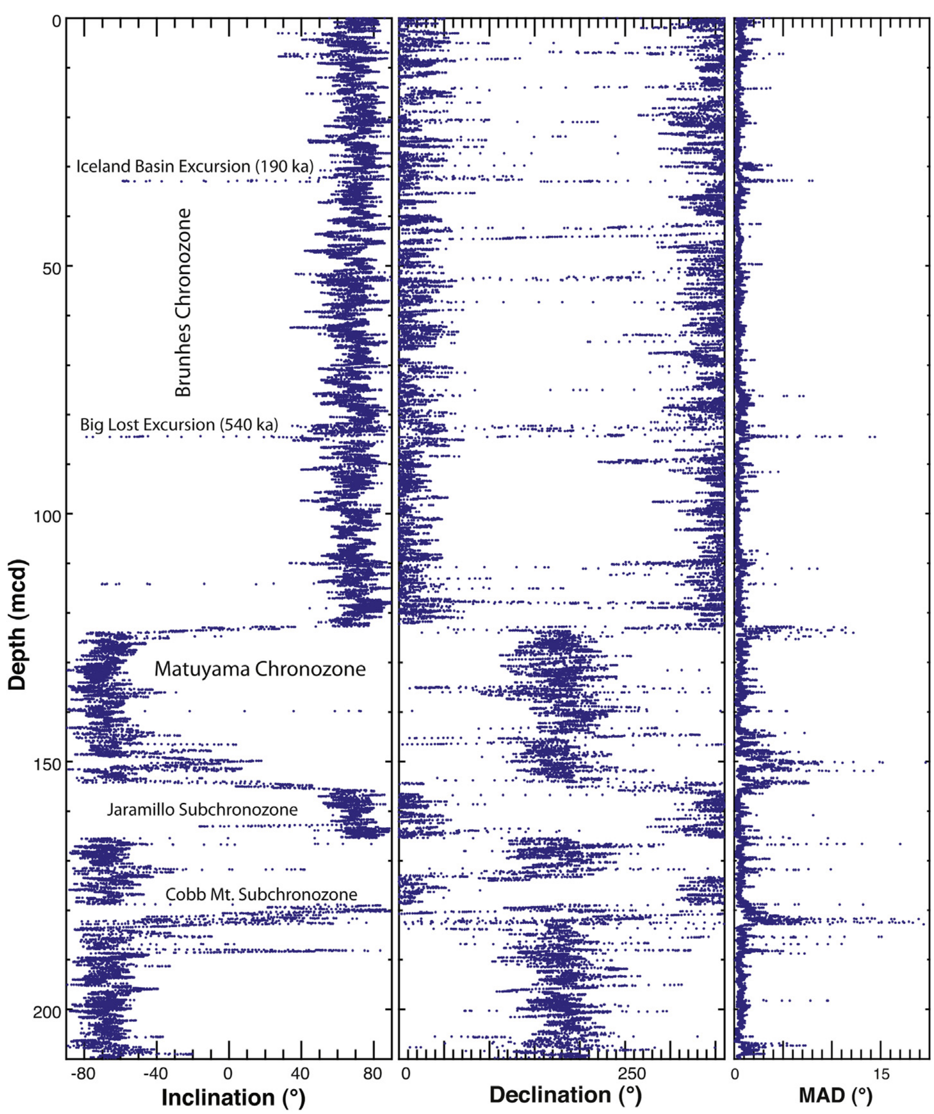

Fig. 2. Site U1306: component declination, inclination and maximum angular deviation (MAD) values computed for the 20–80 mT demagnetization interval, plotted versus depth (meters composite depth, mcd).

Table 1
AMS radiocarbon ages for thirteen samples using specimens of *Neogloboquadrina pachyderma*, sin. UC# refers to the sample number at the W. M. Keck Carbon Cycle Accelerator Mass Spectrometry Laboratory at UC Irvine.

Sample	Depth (mcd)	UC#	Fraction modern	±	$\Delta^{14}C$ (‰)	±	^{14}C (ka)	±	Cal. age (yr BP)	±
1306B-1-1 1-3	0.01	49455	0.5151	0.0008	−484.9	0.8	5330	15	5644	16
1306B-1-1 36-38#1	0.36	49463	0.5564	0.0008	−443.6	0.8	4710	15	4854	7
1306B-1-1 36-38#2	0.36	49464	0.4734	0.0010	−526.6	1.0	6010	20	6385	25
1306A-1-1 81-83	0.81	49456	0.2165	0.0007	−783.5	0.7	12,295	25	13,731	44
1306A-1-1121-123#1	1.21	49465	0.1266	0.0007	−873.4	0.7	16,600	45	19,327	79
1306A-1-1121-123#2	1.21	49466	0.1209	0.0010	−879.1	1.0	16,970	70	19,686	96
1306A-1-2 16-18	1.66	49457	0.0914	0.0006	−908.6	0.6	19,220	60	22,403	80
1306A-1-2 41-43	1.91	49458	0.2926	0.0007	−707.4	0.7	9875	20	10,715	27
1306A-1-2 86-88#1	2.36	49467	0.0781	0.0007	−921.9	0.7	20,480	70	23,990	106
1306A-1-2 86-88#2	2.36	49468	0.0716	0.0010	−928.4	1.0	21,190	120	24,824	211
1306A-1-3 51-53	3.51	49459	0.0490	0.0006	−951.0	0.6	24,220	110	28,532	184
1306A-1-4106-108,111-113#1	5.56	49469	0.0426	0.0006	−957.4	0.6	25,350	130	29,956	248
1306A-1-4106-108,111-113#2	5.56	49470	0.0362	0.0010	−963.8	1.0	26,670	230	31,523	287

assessment of the quality of the directional record (Fig. 2). Declinations were adjusted for vertical-axis core rotation by uniform rotation of each core so that the mean declination for each core is oriented north or south for positive and negative inclination intervals, respectively (Fig. 2).

The magnetic properties of Quaternary sediments on Eirik Drift are dominated by magnetite (Stoner et al., 1995, 1996; Evans et al., 2007; Kawamura et al., 2012; Mazaud et al., 2012). The mean S-ratio in the Brunhes Chron at Site U1306 is 0.96 with a standard deviation of 0.15, similar to values observed at Site U1305 (Mazaud et al., 2012). S-ratios close to unity indicate that the magnetic properties are dominated by low-coercivity magnetic minerals.

Following the calibration of κ_{ARM} versus κ of King et al. (1983), the Site U1306 magnetite grain-size lies in the vicinity of 0.1–5 μm, depending on the peak alternating field used to demagnetize the ARM (Fig. 3a). The linearity of the distributions in Fig. 3a implies a restricted grain-size range, that is apparently finer and more restricted than at Site U1305 where magnetite grain sizes are in the 1–20 μm range based on κ_{ARM}/κ and hysteresis measurements (Mazaud et al., 2012).

The hysteresis ratio plot of Day et al. (1977) provides an alternative means of assessing magnetite grain size. Hysteresis data for Site U1306, collected from each 150-cm section in the composite splice, are confined to the PSD field of the Day plot (Fig. 3b). The data lie close to the theoretical magnetite grain size mixing line (Carter-Stiglitz et al., 2001; Dunlop and Carter-Stiglitz, 2006) and, by comparison with empirical hysteresis ratios from sized (unannealed) magnetite (Dunlop, 2002), the grain sizes lie in the 1–5 μm grain-size range (Fig. 3b). Comparison of Fig. 3a and b indicates that the two magnetic grain size estimates are most consistent for κ_{ARM} values after demagnetization at peak fields of 20 mT. Note that magnetic grain size that may not be simply related to non-magnetic grain size (e.g., Hatfield et al., 2013).

The gradients of IRM acquisition curves plotted on a logarithmic applied-field scale can be modeled in terms of two coercivity populations in the 30–50 mT range (Fig. 4a), which suggests that fine-grained magnetite is the principal magnetic mineral. FORC diagrams also indicate limited spreading along the B_u axis, and are compatible with fine-grained magnetite with coercivities extending up to ~80 mT (Fig. 4b). Note that the upper and lower diagrams in Fig. 4 are from glacial and interglacial marine isotope stages, respectively, and are similar, indicating that the magnetic contrast between glacial and interglacial stages is subtle, an inference consistent with observations from Fig. 3.

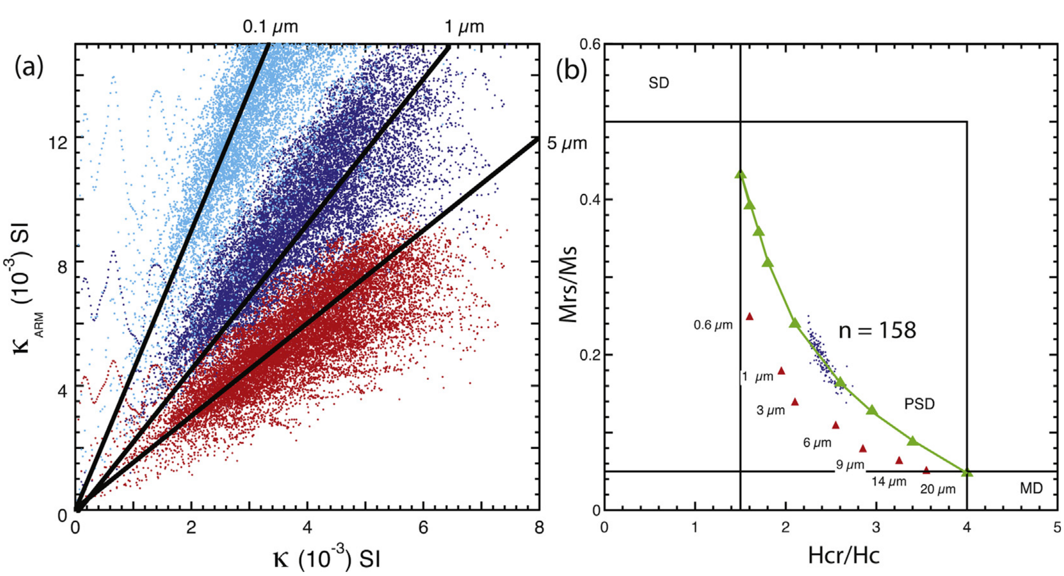

Fig. 3. Site U1306: (a) volume susceptibility (κ) versus anhysteretic susceptibility (κ_{ARM}) before AF demagnetization of anhysteretic remanent magnetization (ARM) (light blue) and after ARM demagnetization at peak fields of 20 mT (dark blue) and 30 mT (red), with the magnetite grain-size calibration after King et al. (1983). (b) Hysteresis ratio plot from Day et al. (1977) for each core section from the composite splice of Site U1306 (blue dots, $n = 158$) with a theoretical magnetite grain size mixing line (green triangles) and data from sized (unannealed) magnetite (red triangles) (see text for references). (For interpretation of the references to color in this figure legend, the reader is referred to the web version of this article.)

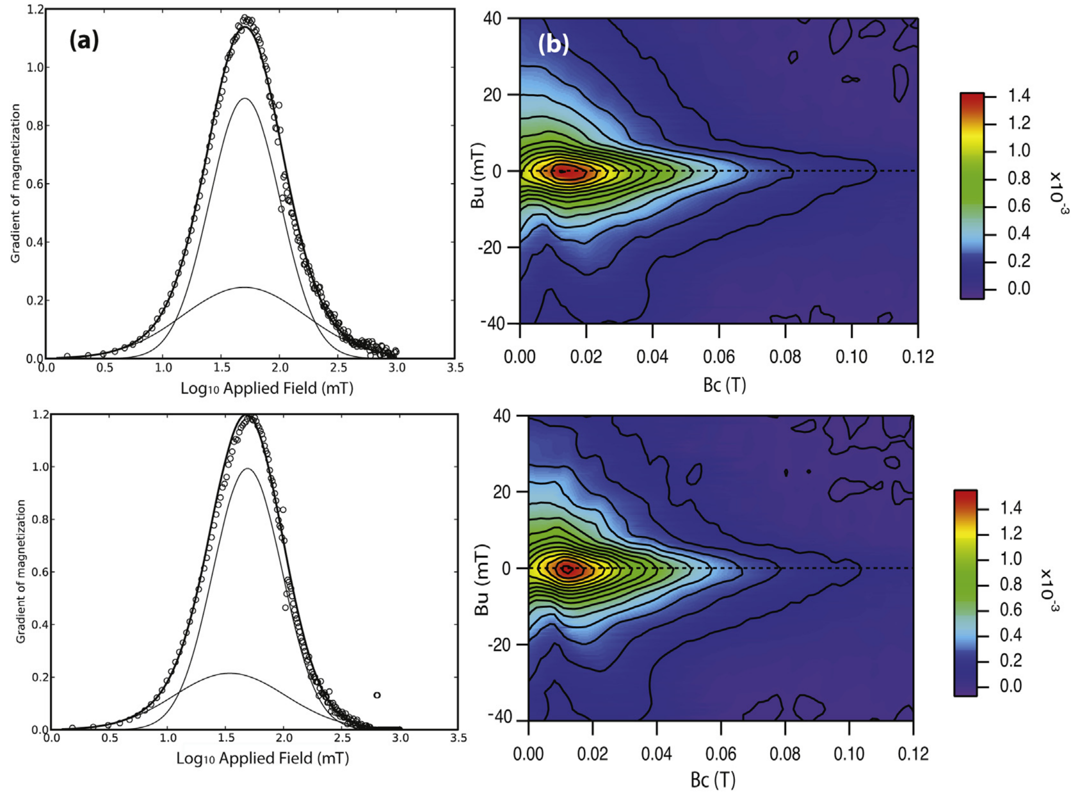

Fig. 4. Site U1306: (a) first derivatives (gradients) of IRM acquisition curves (open circles) modeled using a two-component coercivity spectra (thinner lines) to fit the open circles (thicker line). (b) First-order reversal curves (FORCs) with smoothing factor = 6. Upper and lower plots are for samples from glacial and interglacial marine isotope stages (MIS) 10 and 11, respectively.

TEM observation of a single magnetic extract from 9.5 mcd at Site U1306 demonstrates the presence of irregular-shaped titanomagnetites in the 0.1 μm to few-μm grain size range (Fig. 5). EDS elemental analyses of multiple grains reveal Fe, O and Ti, as the only detectable elements (Fig. 5) implying, along with their irregular outlines, that these titanomagnetite grains are detrital in origin. No biogenic magnetite grains, easily distinguished from detrital grains by their shape, size, and absence of Ti (see Channell et al., 2013), were observed on the TEM grid.

In Fig. 6, we plot slopes of NRM/ARM, NRM/ARMAQ and NRM/IRM, and associated r-values for the 20–60 mT peak demagnetization/acquisition field. ARMAQ data were not acquired for the 0–35 mcd interval, as ARMAQ did not become part of our standard laboratory protocol until after this upper interval had been measured. The NRM/ARM and NRM/ARMAQ paleointensity proxies at Site U1306 are consistent, and linear correlation coefficients (r) are close to unity, indicating that the slopes are well defined within the chosen (20–60 mT) demagnetization interval. The NRM/IRM record is associated with many r-values below 0.98, probably due to the greater effect of coarse magnetite grains (that do not contribute significantly to NRM) on IRM relative to ARM. For age model purposes, we utilize only the NRM/ARM RPI proxy, which closely matches the NRM/ARMAQ proxy where available.

4. Age model

The Site U1306 RPI and planktic δ^{18}O records, on the tandem age model, are plotted together with the PISO RPI stack (Fig. 7) and the LR04 δ^{18}O template (Fig. 8). In Figs. 7 and 8, we also show (as dashed blue lines) the correlation based on an "initial" visual match of the δ^{18}O record to LR04, without knowledge of the RPI record, but cognizant of polarity reversals. For δ^{18}O data (Fig. 8), the "initial" and "tandem" age models yield similar (Pearson) correlation coefficients (to LR04) with slightly lower values for the "tandem" age model than for the "initial" age model (0.66 and 0.68, respectively). For the RPI data (Fig. 7), the two age models yield different correlation coefficients, indicating (understandably) a better RPI fit for the "tandem" than for the "initial" age model (0.78 and 0.41, respectively).

The tandem age model is broadly compatible with the thirteen AMS radiocarbon ages for the 6–31 ka interval (Table 1, Fig. 9). Four samples were analyzed twice using successive leaching. An age inversion is apparent for sample 1306A-1-2, 41–43 cm (1.91 mcd). There is no indication that there were problems with this AMS ^{14}C determination, and we suspect that this anomaly may result from something as mundane and a mislabeled sample. The radiocarbon ages were not used as age-ties in "tandem" age model, but are broadly consistent with it (Fig. 9).

5. Discussion

Based on correlation coefficients given above, as well as the ages of apparent excursions (Fig. 2), tandem correlation of δ^{18}O and RPI to calibrated templates (LR04 and PISO) appears to provide an improved age model compared to that based on traditional use of δ^{18}O alone (Figs. 7 and 8). At Site U1306, the RPI record extends beyond the planktic δ^{18}O record, and here (1–1.5 Ma) the age model utilizes only RPI. The process of tandem correlation not only improves age model resolution, by providing more δ^{18}O/RPI features that can be correlated, it also provides a check on planktic δ^{18}O that can be perturbed by local to regional surface water anomalies (e.g.

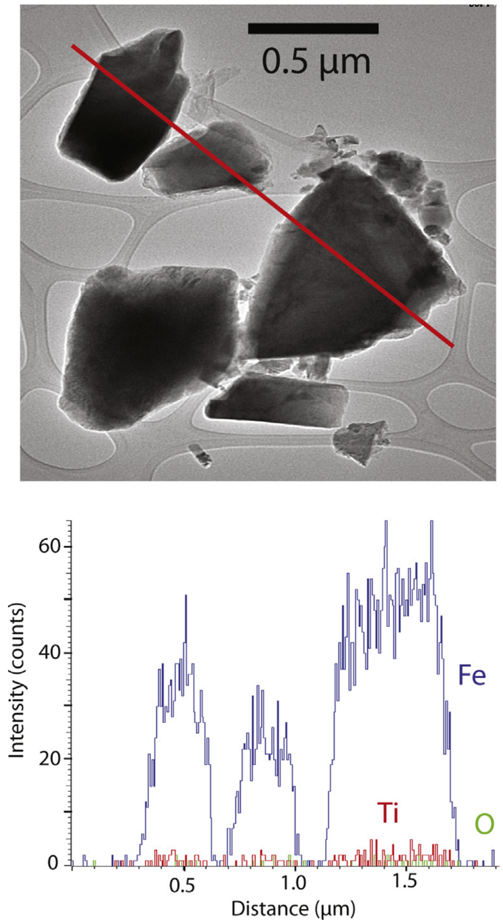

Fig. 5. TEM micrograph of detrital titanomagnetite grains from 9.5 mcd at Site U1306. Red line indicates the position of a 1.9 µm-long energy dispersive x-ray spectroscopy (EDS) line-scan, with plot of intensity for Fe, O and Ti versus distance along that line.

meltwater) that could result in erroneous correlations to the global ice-volume signal.

Tandem age models result in the recognition of low $\delta^{18}O$ values preceeding glacial terminations that are generally not recognized in the age model utilizing $\delta^{18}O$ alone (blue dashed line in Fig. 8). Subtracting the Site U1306 $\delta^{18}O$ values from the LR04 $\delta^{18}O$ provides a crude means of subtracting the ice-volume signal from the Site U1306 $\delta^{18}O$ record thereby revealing the surface-water (e.g. meltwater) anomalies prior to Terminations I, III, IV, V, VII, VIII, IX and X (Fig. 10). Support for this interpretation comes from susceptibility and κ_{ARM}/κ values sensitive to magnetic concentration and magnetic grain-size, respectively, particularly within MIS 10 and 12 (shaded in Fig. 11), that indicate "glacial" values (relatively high susceptibility and magnetic grain size) during the interval with light $\delta^{18}O$ values prior to Terminations IV and V.

The Site U1305 (Fig. 1) age model of Hillaire-Marcel et al. (2011) utilizes 29 $\delta^{18}O$ ties to LR04 and three polarity reversals from shipboard magnetic results (Expedition 303 Scientists, 2006b) over the last 1.1 Myr. The tandem correlations at Site U1306 produce sedimentation rates that are more continuous than age models based on a discrete number of tie lines as at Site U1305 (Fig. 12). At Site U1305, according to the age model of Hillaire-Marcel et al. (2011), sedimentation rates were elevated during interglacial stages, either during peak interglacials or during glacial transitions from peak interglacials, and sedimentation rates were at a minimum during peak glacials (Fig. 12). At Site U1306, the sedimentation rate pattern is different, with peaks in sedimentation rate during glacials or glacial inceptions, and minima during interglacials (Fig. 12). This general pattern appears to be maintained throughout the ~1.5 Myr record at Site U1306.

The MIS 21-22 interval is marked by highly variable $\delta^{18}O$ values at Site U1306 (Fig. 8), indicating surface-water $\delta^{18}O$ anomalies prior to Termination X (Fig. 10), that occur within an interval of elevated sedimentation rate in MIS 22 (Fig. 12). The MIS 21–22

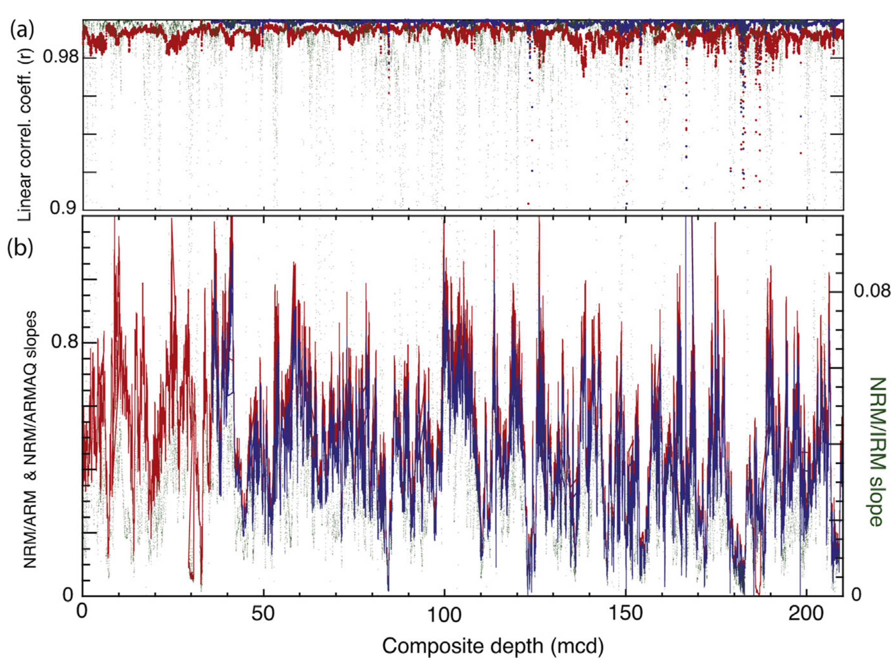

Fig. 6. Site U1306 relative paleointensity (RPI) proxies: (a) linear correlation coefficients (r) for slopes of NRM/ARM (red), NRM/ARMAQ (blue) and NRM/IRM (green dots), (b) Slopes of NRM/ARM (red), NRM/ARMAQ (blue) and NRM/IRM (green dots) for the 20–60 mT demagnetization and acquisition interval. NRM/ARMAQ not measured for the uppermost part of the record. (For interpretation of the references to color in this figure legend, the reader is referred to the web version of this article.)

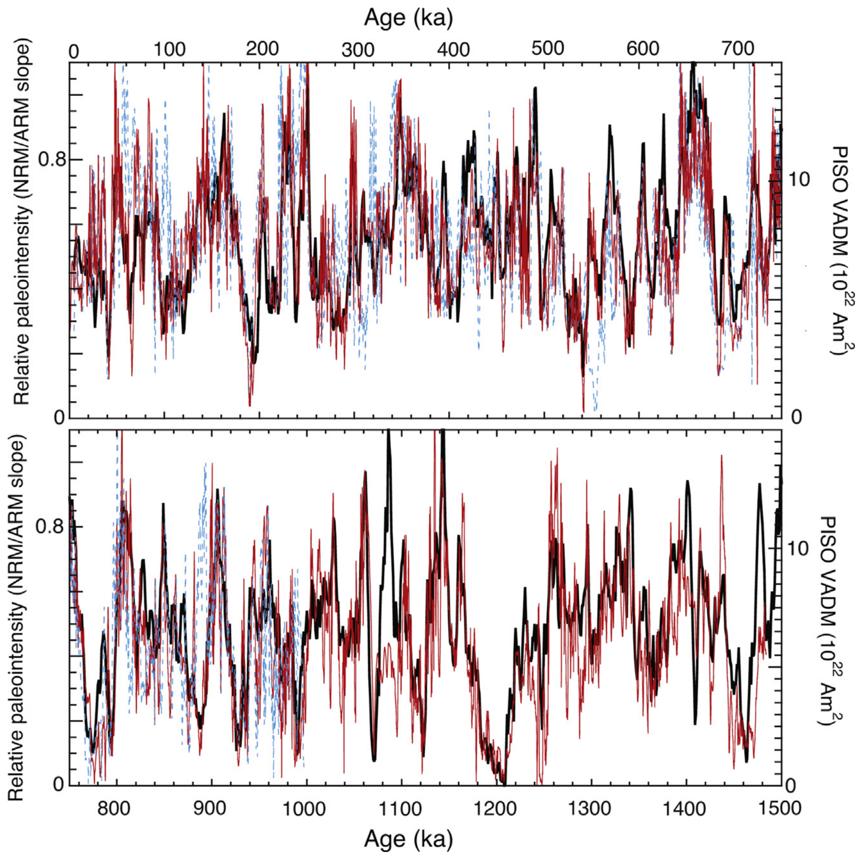

Fig. 7. Site U1306 relative paleointensity (RPI) proxy (red, slope of NRM/ARM) placed on the tandem age model compared with the same data placed on the initial age model based on $\delta^{18}O$ alone (dashed blue line), compared to the PISO RPI stack (black; Channell et al., 2009). (For interpretation of the references to color in this figure legend, the reader is referred to the web version of this article.)

interval immediately postdates the onset of the mid-Pleistocene transition (MPT) at MIS 22 time (Elderfield et al., 2012) and the anomalous $\delta^{18}O$ values may denote changes in the activity of the DWBC and/or changes in surface waters due to early deglaciation on Greenland.

At Site U1306, magnetite grain size (κ_{ARM}/κ) tends to be finer and concentration (susceptibility) tends to be lower during interglacial stages, and coarsening and increased concentration (susceptibility) is associated with glacial inceptions (Fig. 11), possibly coincident with shoaling of the DWBC. This is the opposite of the pattern at Site U1305 where interglacial stages are associated with a marked increase in both magnetic susceptibility and magnetite grain size (Mazaud et al., 2012). At Site U1306, discrete low-susceptibility features, characterized by low ARM intensity and low magnetic grain size, denoted by κ_{ARM}/κ maxima, occur largely within interglacial stages (Fig. 11). Many of these low-susceptibility, low ARM intensity, features correlate with peaks in the wt% >63 μm fraction, implying intervals rich in coarse carbonate fragments, including foraminifera, possibly formed by winnowing.

The DWBC is presently active in the ~2000–3000 m water depth range, eroding sediments along the eastern edge of the Eirik Drift and depositing sediment at the toe of the drift, in the vicinity of Site U1305 (Hunter et al., 2007a). Higher sedimentation rates at Site U1305 during interglacials (Fig. 12b), associated with higher magnetic susceptibility and magnetite grain size (Mazaud et al., 2012), implies that the DWBC was more active during Quaternary interglacials when it continued to supply detritus to Site U1305. The depth and/or velocity associated with the DWBC was apparently different during Quaternary glacial intervals, when it may have slowed and shoaled possibly due to lowered salinity, ceasing to supply the same amount of detritus to Site U1305 and enhancing deposition at Site U1306 where glacial deposition may also have been augmented by near-surface currents (EGC and EGCC) and ice-rafted debris. Inferred glacial/interglacial fluctuations in vigor and depth of the DWBC across Eirik Drift are consistent with observations on the Blake-Bahama Outer Ridge where shoaling and reduced DWBC vigor are associated with glacial intervals (Haskell et al., 1991; Bianchi et al., 2001; Yokokawa and Franz, 2002).

6. Conclusions

Ice cores from the poles have provided, arguably, the most important records of Quaternary climate, in large part because of unprecedented chronological resolution. Marine sediment records of climate/environmental change are, unlike ice cores, widely distributed and available over long timescales, but they have relatively low stratigraphic resolution. Improving the resolution of marine Quaternary stratigraphy is a major challenge because leads-and-lags in the climate system are difficult to resolve without it. The traditional tool of marine Quaternary stratigraphy, oxygen isotopes ($\delta^{18}O$), is perturbed by temperature and water chemistry, and is not purely a global (ice-volume) signal even in benthic foraminifera. Relative paleointensity (RPI), on the other hand, should be a global signal when recorded by sediments with mean sedimentation rates less then a few-decimeters/ka because the non-axial dipole components of the geomagnetic

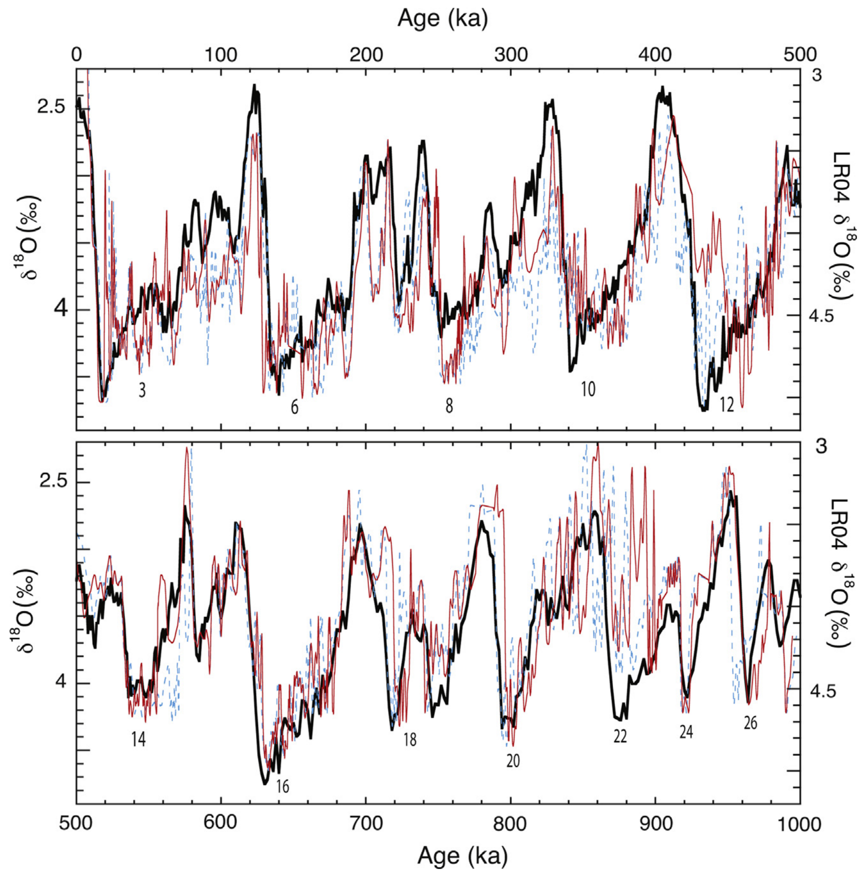

Fig. 8. Site U1306 planktic oxygen isotope record ($\delta^{18}O$) with 7-point gaussian smoothing (red) placed on the tandem age model compared with the same data placed on the initial age model based on $\delta^{18}O$ alone (dashed blue line), compared to the LR04 calibrated template (black; Lisiecki and Raymo, 2005). Certain (glacial) marine isotope stages are labeled. (For interpretation of the references to color in this figure legend, the reader is referred to the web version of this article.)

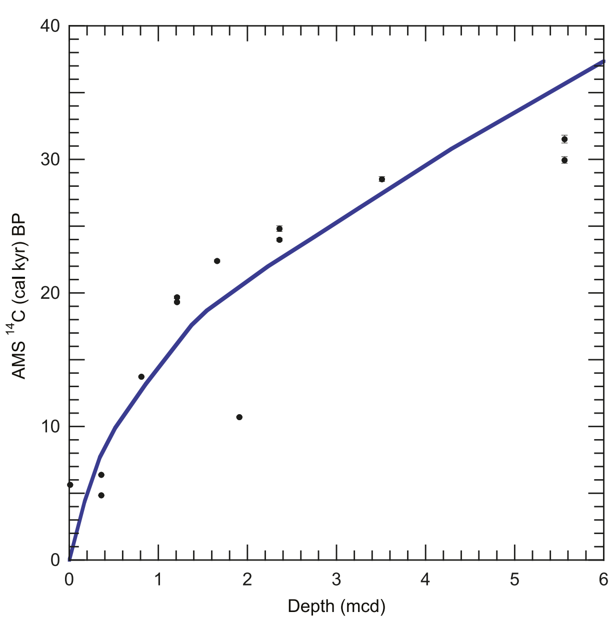

Fig. 9. Age-depth comparison for the AMS radiocarbon ages (black symbols with age-error bars hardly visible, Table 1) and for the Site U1306 tandem age model (blue line) that does not involve the radiocarbon ages. (For interpretation of the references to color in this figure legend, the reader is referred to the web version of this article.)

field are believed to average out on multi-centennial timescales (e.g. Lhuillier et al., 2011). The problem, of course, is that RPI recording in sediments is not infallible, and is often influenced by lithology and hence environmental factors. Apart from using magnetic criteria to select sediments appropriate for RPI studies, including tests for SD/PSD magnetite and restricted magnetite grain size (Figs. 3 and 4), we assess the usefulness of RPI by constructing "tandem" age models that utilize both $\delta^{18}O$ and RPI. Internally-consistent $\delta^{18}O$/RPI age models provide a "test of concept" in the application of RPI as a chronological tool. In the future, the use of RPI alone may free $\delta^{18}O$ from its chronological role, and allow $\delta^{18}O$ to be interpreted in terms of its regional environmental signal.

Using IODP Site U1306 as an example, we conclude that RPI can augment $\delta^{18}O$ in age model construction, and in this case, the "tandem" age model provides an internally-consistent age model that "adds value" to the age model generated by $\delta^{18}O$ alone. Low (light) values of $\delta^{18}O$ that precede glacial terminations, attributed to regional surface water affects, are an outcome from the "tandem" age model that would not be apparent using $\delta^{18}O$-based age models. Light values of $\delta^{18}O$ at Site U1306 provide evidence for "early" deglaciation on Greenland prior to glacial Terminations I, III, IV, V, VII, VIII, IX and X. In addition, the "tandem" age models provide smoothly varying sedimentation-rate maps that provide higher resolution sedimentation rate estimates on Eirik Drift. At Site U1306, close to the crest of the drift, higher sedimentation-rate intervals, accompanied by greater magnetic concentration and grain size, are associated with glacial intervals. In contrast, at Site

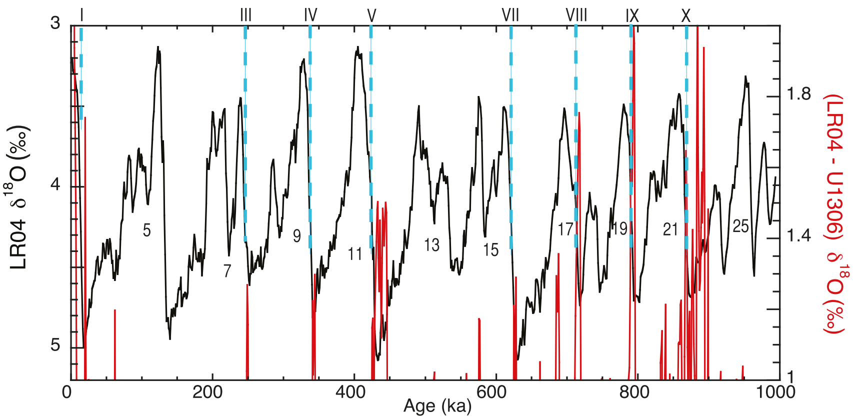

Fig. 10. Anomalies in surface water $\delta^{18}O > 1‰$ (red) determined by subtracting the Site U1306 planktic $\delta^{18}O$ from the LR04 $\delta^{18}O$ "ice-volume" signal, compared with the LR04 $\delta^{18}O$ stack (black; Lisiecki and Raymo, 2005). Terminations (Roman numerals and dashed blue lines), and interglacial isotopic stages, are labeled. (For interpretation of the references to color in this figure legend, the reader is referred to the web version of this article.)

U1305, located 191 km SW of Site U1306 in the deep-water toe of the drift, increased depth (and vigor) of the DWBC resulted in elevated deposition, and elevated magnetic concentration and grain size, during interglacials. The contrasting glacial/interglacial depositional pattern at the two sites appears to have persisted for the last ~1.5 Myrs, spanning the MPT. The Quaternary architecture of the Eirik Drift is intimately related to the variable activity of the DWBC as a principal component of AMOC.

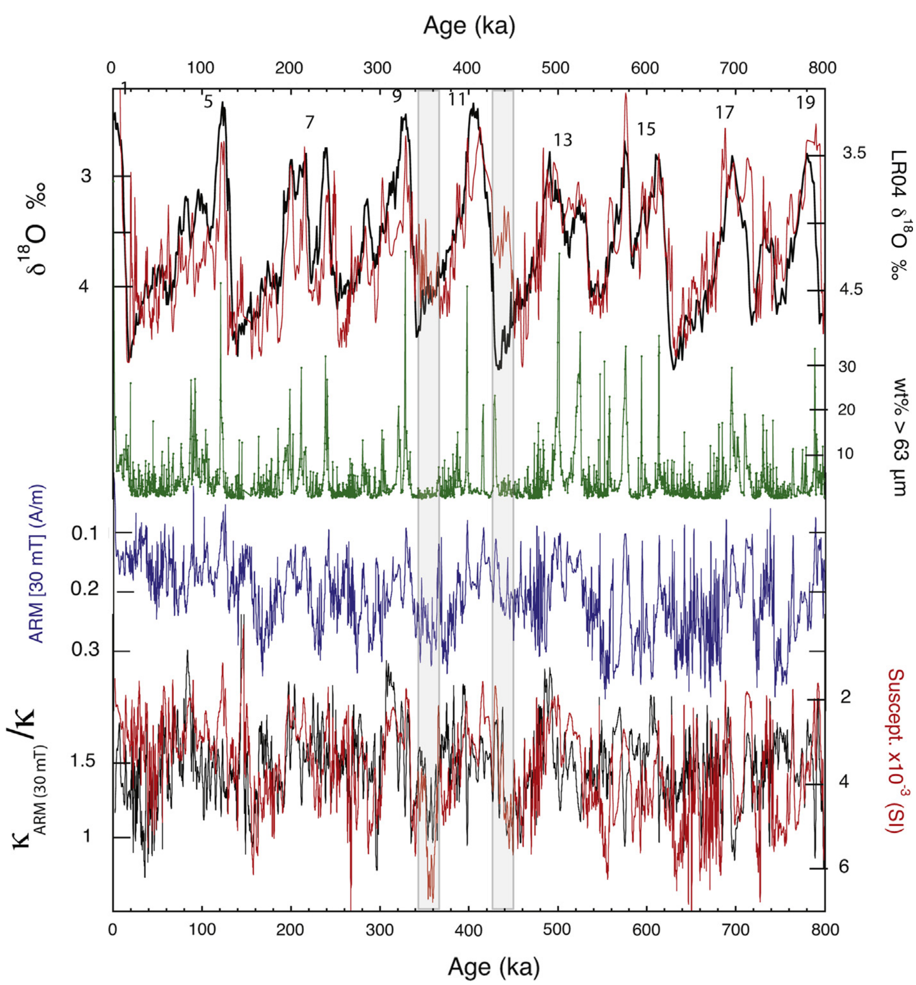

Fig. 11. Site U1306 magnetic grain size proxy (κ_{ARM}/κ) after 30 mT peak field demagnetization of ARM, volume susceptibility, ARM intensity after 30 mT peak field demagnetization, wt% >63 μm fraction, aligned with planktic oxygen isotope record (red) and LR04 $\delta^{18}O$ calibrated template (black; Lisiecki and Raymo, 2005). Low values of $\delta^{18}O$ in MIS 10 and 12 (shaded), correspond to high (glacial) values of susceptibility and coarse magnetic grain size. Interglacial marine isotope stages are labeled. (For interpretation of the references to color in this figure legend, the reader is referred to the web version of this article.)

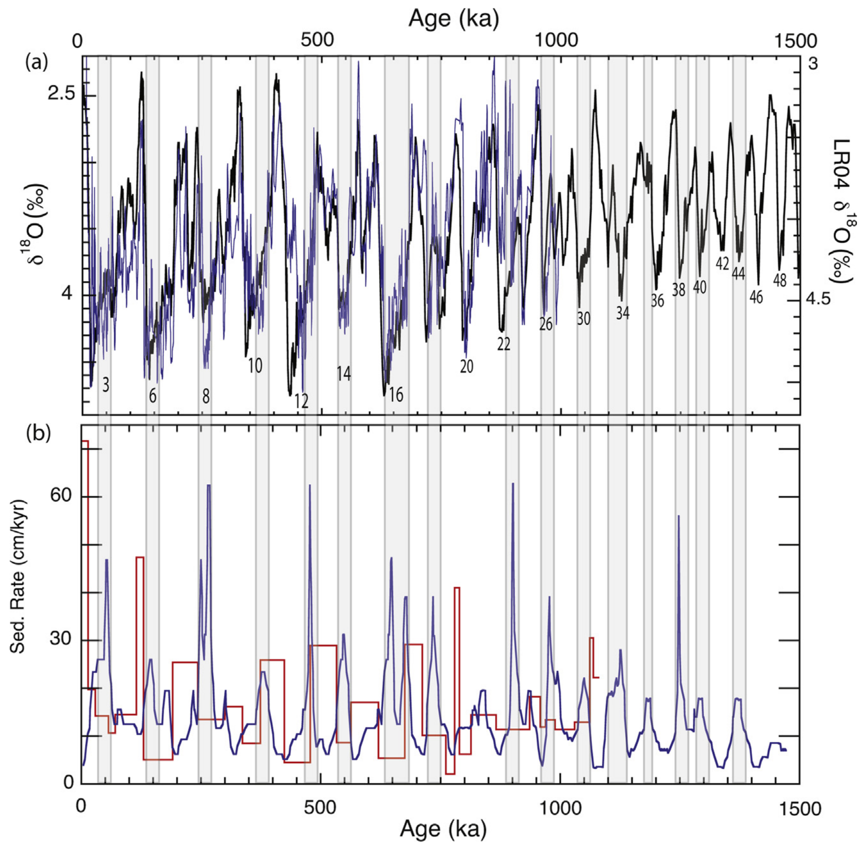

Fig. 12. (a) Planktic oxygen isotope record from Site U1306 (blue) and LR04 $\delta^{18}O$ calibrated template (black; Lisiecki and Raymo, 2005). Certain (glacial) marine isotope stages are labeled. (b) Site U1306 sedimentation rates (blue) based on the tandem age model compared to Site U1305 sedimentation rates (red) from the $\delta^{18}O$ age model of Hillaire-Marcel et al. (2011). Higher sedimentation rate intervals (corresponding to glacials) at Site U1306 are shaded. (For interpretation of the references to color in this figure legend, the reader is referred to the web version of this article.)

Acknowledgments

We would like to thank the crew and scientists aboard the RV *JOIDES Resolution* during IODP Exp. 303/306, the IODP support staff, and the staff of the Bremen Core Repository. We thank K. Huang for laboratory assistance. This research was supported by US National Science Foundation Grants OCE-0850413 and EAR-1014506 to J.C.

References

Arthur, M.A., Srivastava, S.P., Kaminski, M., Jarrard, R., Osler, J., 1989. Seismic stratigraphy and history of deep circulation and sediment drift development in Baffin Bay and the Labrador Sea. In: Srivastava, S.P., Arthur, M.A., Clement, B., et al. (Eds.), Proc. ODP, Sci. Results, 105. Ocean Drilling Program, College Station, TX, pp. 957–988.

Bacon, S., 1997. Circulation and fluxes in the North Atlantic between Greenland and Ireland. J. Phys. Oceanogr. 27, 1420–1435.

Bacon, S., Saunders, P.M., 2010. The deep western boundary current at cape farewell: results from a moored current meter array. J. Phys. Oceanogr. 40, 815–829.

Banerjee, S.K., Mellema, J.P., 1974. A new method for the determination of paleointensity from the ARM properties of rocks. Earth Planet Sci. Lett. 23, 177–184.

Bé, A.W.H., Tolderlund, D.S., 1971. Distribution and ecology of living planktonic foraminifera in surface waters of the Atlantic and Indian oceans. In: Funnel, B.M., Riedel, W.R. (Eds.), The Micropaleontology of Oceans. Cambridge University Press, Cambridge, pp. 105–149.

Bianchi, G.G., Vautravers, M., Shackleton, N.J., 2001. Deep flow variability under apparently stable North Atlantic Deep Water production during the last interglacial of the subtropical NW Atlantic. Paleoceanography 16, 306–316.

Butzin, M., Prange, M., Lohmann, G., 2005. Radiocarbon simulations for the glacial ocean: the effects of wind stress, Southern Ocean sea ice and Heinrich events. Earth Planet. Sci. Lett. 235, 45–61.

Carter-Stiglitz, B., Moskowitz, B., Jackson, M., 2001. Unmixing magnetic assemblages and the magnetic behavior of bimodal mixtures. J. Geophys. Res. 106, 26,397–26,411.

Channell, J.E.T., Mazaud, A., Sullivan, P., Turner, S., Raymo, M.E., 2002. Geomagnetic excursions and paleointensities in the 0.9–2.15 Ma interval of the Matuyama Chron at ODP Site 983 and 984 (Iceland Basin). J. Geophys. Res. 107 (B6). http://dx.doi.org/10.1029/2001JB000491.

Channell, J.E.T., Kanamatsu, T., Sato, T., Stein, R., Alvarez Zarikian, C.A., Malone, M.J., the Expedition 303/306 Scientists, 2006. North Atlantic Climate, Expeditions 303 and 306 of the Riserless Drilling Platform from St. John's, Newfoundland, to Ponta Delgada, Azores (Portugal), Sites U1302–u1308, 25 September–17 November 2004 and from Ponta Delgada, Azores (Portugal) to Dublin, Ireland, Sites U1312–U1315, 2 March–26 April 2005. Integrated Ocean Drilling Program Management International, Inc. for the Integrated Ocean Drilling Program. Available at: http://iodp.tamu.edu/publications/exp303_306/30306title.htm.

Channell, J.E.T., Hodell, D.A., Xuan, C., Mazaud, A., Stoner, J.S., 2008. Age calibrated relative paleointensity for the last 1.5 Myr at IODP Site U1308 (North Atlantic). Earth Planet. Sci. Lett. 274, 59–71.

Channell, J.E.T., Xuan, C., Hodell, D.A., 2009. Stacking paleointensity and oxygen isotope data for the last 1.5 Myrs (PISO-1500). Earth Planet. Sci. Lett. 283, 14–23.

Channell, J.E.T., Hodell, D.A., Romero, O., Hillaire-Marcel, C., de Vernal, A., Stoner, J.S., Mazaud, A., Röhl, U., 2012a. A 750-kyr detrital-layer stratigraphy for the North Atlantic (IODP site U1302-U1303, orphan knoll, labrador sea). Earth Planet. Sci. Lett. 317–318, 218–230.

Channell, J.E.T., Hodell, D.A., Curtis, J.H., 2012b. ODP Site 1063 (Bermuda Rise) revisited: oxygen isotopes, excursions and paleointensity in the Brunhes Chron. Geochem. Geophys. Geosyst. 13, Q02001. http://dx.doi.org/10.1029/2011GC003897.

Channell, J.E.T., Hodell, D.A., Margari, V., Skinner, L.C., Tzedakis, P.C., Kesler, M.S., 2013. Biogenic magnetite, detrital hematite, and relative paleointensity in sediments from the Southwest Iberian Margin. Earth Planet. Sci. Lett. 376, 99–109.

Coplen, T.B., 1996. New guidelines for the reporting of stable hydrogen, carbon, and oxygen isotope ratio data. Geochim. Cosmochim. Acta 60, 3359.

Day, R., Fuller, M., Schmidt, V.A., 1977. Hysteresis properties of titanomagnetites: grain-size and compositional dependence. Phys. Earth Planet. Intr. 13, 260–267.

Dunlop, D.J., 2002. Theory and application of the Day plot (M_{rs}/M_s versus H_{cr}/H_c) 1. Theoretical curves and tests using titanomagnetite data. J. Geophys. Res. 107 (B3), 2056. http://dx.doi.org/10.1029/2001JB000486.

Dunlop, D.J., Carter-Stiglitz, B., 2006. Day plots of mixtures of superparamagnetic, single domain, pseudosingle domain, and multidomain magnetites. J. Geophys. Res. 111, B12S09. http://dx.doi.org/10.1029/2006JB004499.

Elderfield, H., Ferretti, P., Greaves, M., Crowhurst, S., McCave, I.N., Hodell, D.A., Piotrowski, A.M., 2012. Evolution of ocean temperature and ice volume through the Mid-Pleistocene climate transition. Science 337, 704–709.

Expedition 303 Scientists, 2006a. Site U1306. In: Channell, J.E.T., Kanamatsu, T., Sato, T., Stein, R., Alvarez Zarikian, C.A., Malone, M.J. (Eds.), Expedition 303/306 Scientists, Proc. IODP, 303. Integrated Ocean Drilling Program Management International, Inc., College Station TX http://dx.doi.org/10.2204/iodp.proc.303306.103.2006.

Expedition 303 Scientists, 2006b. Site U1305. In: Channell, J.E.T., Kanamatsu, T., Sato, T., Stein, R., Alvarez Zarikian, C.A., Malone, M.J. (Eds.), Expedition 303/306 Scientists, Proc. IODP, 303. Integrated Ocean Drilling Program Management International, Inc., College Station TX http://dx.doi.org/10.2204/iodp.proc.303306.103.2006.

Evans, H.F., Channell, J.E.T., Stoner, J.S., Hillaire-Marcel, C., Wright, J.D., Neitzke, L.C., Mountain, G.S., 2007. Paleointensity-assisted chronostratigraphy of detrital layers on the Eirik Drift (North Atlantic) since marine isotope stage 11. Geochem. Geophys. Geosyst. 8, Q11007. http://dx.doi.org/10.1029/2007GC111720.

Fairbanks, R.G., Mortlock, R.A., Chiu, T.-C., Cao, L., Kaplan, A., Guilderson, T.P., Fairbanks, T.W., Bloom, A.L., 2005. Marine radiocarbon calibration curve spanning 0 to 50,000 years B.P based on Paired $^{230}Th/^{234}U/^{238}U$ and ^{14}C dates on pristine corals. Quat. Sci. Revs. 24, 1781–1796.

Fagel, N., Hillaire-Marcel, C., Humblet, M., Brasseur, R., Weis, D., Stevenson, R., 2004. Nd and Pb isotope signatures of the clay-size fraction of Labrador Sea sediments during the Holocene: implications for the inception of the modern deep circulation pattern. Paleoceanography 19, PA3002. http://dx.doi.org/10.1029/2003PA000993.

Hall, I.R., Becker, J., 2007. Deep Western Boundary Current variability in the subtropical northwest Atlantic Ocean during marine isotope stages 12-10. Geochem. Geophys. Geosyst. 8, Q06013. http://dx.doi.org/10.1029/2006GC001518.

Harrison, R.J., Feinberg, J.M., 2008. FORCinel: an improved algorithm for calculating first-order reversal curve distributions using locally weighted regression smoothing. Geochem. Geophys. Geosyst. 9, Q05016. http://dx.doi.org/10.1029/2008GC001987.

Haskell, B.J., Johnson, T.C., Showers, W.J., 1991. Fluctuations in deep western North Atlantic circulation on the Blake Outer Ridge during the last deglaciation. Paleoceanography 6, 21–31.

Hatfield, R.G., Stoner, J.S., Carlson, A.E., Reyes, A.V., Housen, B.A., 2013. Source as a controlling factor on the quality and interpretation of sediment magnetic records from the northern North Atlantic. Earth Planet. Sci. Lett. 368, 69–77.

Heslop, D., Dekkers, M.J., Kruiver, P.P., van Oorschot, I.H.M., 2002. Analysis of isothermal remanent magnetization acquisition curves using the expectation maximization algorithm. Geophys. J. Int. 148, 58–64.

Hillaire-Marcel, C., de Vernal, A., 2008. Stable isotope clue to episodic sea-ice formation in the glacial North Atlantic. Earth Planet. Sci. Lett. 268, 143–150.

Hillaire-Marcel, C., de Vernal, A., Bilodeau, G., Wu, G., 1994. Isotope Stratigraphy, sedimentation rates, deep circulation, and carbonate events in the Labrador Sea during the last ~200 ka. Can. J. Earth Sci. 31, 63–89.

Hillaire-Marcel, C., de Vernal, A., McKay, J., 2011. Foraminifer isotope study of the Pleistocene Labrador Sea, northwest North Atlantic (IODP Sites 1302/03 and 1305), with emphasis on paleoceanographical differences between its "inner" and "outer" basins. Mar. Geol. 279, 188–198. http://dx.doi.org/10.1016/j.margeo.2010.11.001.

Holliday, N.P., Bacon, S., Allen, J., McDonagh, E.L., 2009. Circulation and transport in the western boundary currents at Cape Farewell, Greenland. J. Phys. Oceanogr. 39, 1854–1870.

Hunter, S.E., Wilkinson, D., Louarn, E., McCave, I.N., Rohling, E., Stow, D.A.V., Bacon, S., 2007a. Deep western boundary current dynamics and associated sedimentation on the Eirik Drift, Southern Greenland margin. Deep-Sea Res. I 54, 2036–2066.

Hunter, S.E., Wilkinson, D., Stow, D.A.V., Bacon, S., Rohling, E.J., Stanford, J., Kenyon, N.H., Akhemetzhanov, A., 2007b. The eirik drift: a longterm barometer of North Atlantic deep water flux south of cape farewell, Greenland. In: Viana, A., Rebesco, M.L. (Eds.), Economic and Paleoceanographic Significance of Contourite Deposits, Geol. Soc. Spec. Publ., 276, pp. 245–264.

Kawamura, N., Ishikawa, N., Torii, M., 2012. Diagenetic alteration of magnetic minerals in Labrador Sea sediments (IODP Sites U1305, U1306, and U1307). Geochem. Geophys. Geosyst. 13, Q08013. http://dx.doi.org/10.1029/2012GC004213.

King, J.W., Banerjee, S.K., Marvin, J., 1983. A new rock-magnetic approach to selecting sediments for geomagnetic paleointensity studies: application to paleointensity for the last 4000 years. J. Geophys. Res. 88, 5911–5921.

Kirschvink, J.L., 1980. The least squares lines and plane analysis of palaeomagnetic data. Geophys. J. R. Astron. Soc. 62, 699–718.

Levi, S., Banerjee, S.K., 1976. On the possibility of obtaining relative paleointensities from lake sediments. Earth Planet. Sci. Lett. 29, 219–226.

Lhuillier, F., Fournier, A., Hulot, G., Aubert, J., 2011. The geomagnetic secular-variation timescale in observations and numerical dynamo models. Geophys. Res. Lett. 38, L09306. http://dx.doi.org/10.1029/2011GL047356.

Lisiecki, L.E., Lisiecki, P.A., 2002. Application of dynamic programming to the correlation of paleoclimate records. Paleoceanography 17, 1049. http://dx.doi.org/10.1029/2001PA000733.

Lisiecki, L.E., Raymo, M.E., 2005. A Pliocene–Pleistocene stack of 57 globally distributed benthic $\delta^{18}O$ records. Paleoceanography 20, PA1003. http://dx.doi.org/10.1029/2004PA001071.

Lisiecki, L.E., Raymo, M.E., 2009. Diachronous benthic $\delta^{18}O$ responses during late Pleistocene terminations. Paleoceanography 24, PA3210. http://dx.doi.org/10.1029/2009PA001732.

Mazaud, A., Channell, J.E.T., Stoner, J.S., 2012. Relative paleointensity and environmental magnetism since 1.2 Ma at IODP Site U1305 (Eirik Drift, NW Atlantic). Earth Planet. Sci. Lett. 357–358, 137–144.

Muxworthy, A.R., Roberts, A.P., 2007. First-order reversal curve (FORC) diagrams. In: Gubbins, D., Herrero-Bervera, E. (Eds.), Encyclopedia of Geomagnetism and Paleomagnetism. Springer, Dordrecht, Netherlands, pp. 266–272.

Pike, C.R., Roberts, A.P., Verosub, K.L., 1999. Characterizing interactions in fine magnetic particle systems using first order reversal curves. J. Appl. Phys. 85, 6660–6667. http://dx.doi.org/10.1063/1.370176.

Roberts, A.P., Pike, C.R., Verosub, K.L., 2000. First-order reversal curve diagrams: a new tool for characterizing the magnetic properties of natural samples. J. Geophys. Res. 105, 28,461–28,475. http://dx.doi.org/10.1029/2000JB900326.

Robertson, D.J., France, D.E., 1994. Discrimination of remanence-carrying minerals in mixtures, using isothermal remanent magnetization acquisition curves. Phys. Earth Planet. Intr. 84, 223–234.

Skinner, L.C., Shackleton, N.J., 2005. An Atlantic lead over Pacific deep-water change across termination I: implications for the application of the marine isotope stage stratigraphy. Quat. Sci. Rev. 24, 571–580.

Stanford, J.D., Rohling, E.J., Bacon, S., Holliday, N.P., 2011. A review of the deep and surface currents around Eirik Drift, south of Greenland: comparison of the past with the present. Glob. Planet. Change 79, 244–254.

Stoner, J.S., Channell, J.E.T., Hillaire-Marcel, C., 1995. Late Pleistocene relative geomagnetic paleointensity from the deep Labrador Sea: regional and global correlations. Earth Planet. Sci. Lett. 134, 237–252.

Stoner, J.S., Channell, J.E.T., Hillaire-Marcel, C., 1996. The magnetic signature of rapidly deposited detrital layers from the deep Labrador Sea: relationship to North Atlantic Heinrich layers. Paleoceanography 11, 309–325.

Stoner, J.S., Channell, J.E.T., Hillaire-Marcel, C., 1998. A 200 kyr geomagnetic chronostratigraphy for the Labrador Sea: indirect correlation of the sediment record to SPECMAP. Earth Planet. Sci. Lett. 159, 165–181.

Tauxe, L., 1993. Sedimentary records of relative paleointensity of the geomagnetic field: theory and practice. Rev. Geophys. 31, 319–354.

Thomas, R., Guyodo, Y., Channell, J.E.T., 2003. U-channel track for susceptibility measurements. Geochem., Geophys. Geosyst., 1050. http://dx.doi.org/10.1029/2002GC000454.

Xuan, C., Channell, J.E.T., 2009. UPmag: MATLAB software for viewing and processing u-channel or other pass-through paleomagnetic data. Geochem. Geophys. Geosyst. 10, Q10Y07. http://dx.doi.org/10.1029/2009GC002584.

Yokokawa, M., Franz, S.-O., 2002. Changes in grain size and magnetic fabric at the Blake-Bahama Outer Ridge during the late Pleistocene (marine isotope stages 8–10). Mar. Geol. 189, 123–144.